ARCHITECTURE CIVIL ENGINEERING ENVIRONMENT
The Silesian University of Technology No. 1/2009

# STATE OF THE ART IN MODELLING OF SOIL BEHAVIOUR AT SMALL STRAINS

Maciej GRYCZMAŃSKI *

*Prof.; Faculty of Civil Engineering, The Silesian University of Technology, Akademicka 5, 44-100 Gliwice, Poland
E-mail address: *maciej.gryczmanski@polsl.pl*

Received: 02.02.2009; Revised: 24.02.2009; Accepted: 05.03.2009

Abstract

**The present paper is an attempt at a comprehensive overview of studies on behaviour of overconsolidated soils at small strains. The text has been divided into six sections related to different aspects of the addressed issues.**
**The *first* section provides an introduction. The subject of the *second* section is the phenomenon of abrupt drop of the tangent shear and bulk moduli when increasing corresponding strain invariants in the ranges of their small values. Special attention is paid to evaluating the maximum values of moduli which are constant in a region of very small strains. The *third* section concerns the nature of the above mentioned material properties. The results of the discussed Jardine's experiments indicate that there exist four regions of different soil behaviour around a stable stress point within the admissible state space.The *fourth* section focuses on simple hypoelastic laws for soils describing steep decreasing tangent shear and bulk moduli at small to moderate strains. The *fifth* section presents advanced kinematic hardening elasto-plastic models which take into account, in different ways, strong stress-strain nonlinearity at small deformations. Two models are described in more detail. The first of them is the one surface model of the cryptonym NAHOS 1 and the other is the three surface SH3 one. The conclusion inserted in the latter *sixth* section discusses briefly beneficial outcomes of accounting for small strain nonlinearity phenomenon.**

Streszczenie

**Artykuł niniejszy jest próbą obszernego przeglądu badań nad zachowaniem się prekonsolidowanych gruntów przy małych odkształceniach. Tekst podzielony został na sześć rozdziałów związanych z różnymi aspektami przedmiotowej problematyki. Rozdział *pierwszy* stanowi wprowadzenie. Przedmiotem *drugiego* rozdziału jest zjawisko gwałtownego spadku stycznych modułów ścinania i ściśliwości ze wzrostem korespondujących niezmienników odkształcenia w zakresach ich małych wartości. Specjalna uwaga zwrócona jest na szacowanie maksymalnych wartości modułów, które są stałe w przedziale bardzo małych odkształceń. Rozdział *trzeci* dotyczy natury wspomnianych zjawisk. Wyniki omawianych eksperymentów Jardine'a wskazują na istnienie, wokół ustalonego punktu naprężenia wewnątrz dozwolonej przestrzeni stanu, czterech obszarów różnego zachowania się gruntu. Rozdział *czwarty* skupiony jest na prostych prawach hiposprężystych dla gruntów, opisujących stromy spadek stycznych modułów ścinania i ściśliwości w przedziale od małych do umiarkowanych odkształceń. *Piąty* rozdział przedstawia zaawansowane modele sprężysto-plastyczne o wzmocnieniu kinematycznym, które biorą pod uwagę, w różny sposób, silną nieliniowość związków „naprężenie-odkształcenie" w zakresie małych odkształceń. Dwa z nich opisane są bardziej szczegółowo. Pierwszy z nich, jest jednopowierzchniowym modelem o nazwie NAHOS 1 a drugi trójpowierzchniowym modelem SH3. Podsumowanie zamieszczone w ostatnim *szóstym* rozdziale omawia pokrótce korzyści wynikające z uwzględnienia zjawiska silnej nieliniowości w zakresie małych odkształceń.**

Keywords: **Soil overconsolidation subspace; Steep decrease of shear and bulk moduli at small strains; Kinematic nature of stiffness changes; Simple nonlinear and advanced kinematic hardening elasto-plastic models accounting for strong nonlinearity at small strains.**

## 1. INTRODUCTION

The terms: „soil behaviour at small strains", "small strain stiffness", "small strain nonlinearity" have recently become very important notions of soil mechanics. They all refer to the same phenomenon characteristic for particulate media which consists in an abrupt drop in initially high soil stiffness, while soil deformation increases in a range of small values. It means that the change in distortional strain from $10^{-4}$ to $10^{-2}$ can involve the secant shear modulus reduction exceeding one order of magnitude (from ten to fifteen times.) The "distortional strain-tangent shear modulus" relationship appears to be almost identical in respect of character. The compared curves run beside one another while the distance between them increases slightly (Fig. 1.) The routes of "volumetric strain-bulk. (secant or tangent) modulus" characteristics are also similar to those shown in Fig. 1 but they drop more steeply (Fig. 2).

Since the early eighties many laboratory and field tests have been performed world-wide to study soil behaviour at small strains and describe it mathematically. It is worth noticing that natural soil deposits are practically always more or less overconsolidated. Thus, the first stages of material's responses to loads transmitted from structures run through the overconsolidation state subspace, and the small strain nonlinearity phenomenon is also related to that state. Initially, investigations focused solely on the physical nonlinearity as defined above, without identifying the nature of deformations (reversible or irreversible, and instant or retarded.)

Later studies carried out at the beginning of the nineties were devoted to changes in character of deformations together with their increase, from linear elastic, through nonlinear elastic (hysteretic) and small plastic, to large plastic for normal consolidation states.

At the same time the relevant research work was performed on the constitutive models describing overconsolidated soil behaviour at small strains. The first group of proposals comprised some relatively simple hypoelastic models approximating directly changes in stiffness using hyperbolic or logarithmic functions, and some classical elasto-plastic ones improved by incorporating one or more mentioned empirical formulas describing tangent stiffness moduli, as material functions.

The other group included advanced three-surface kinematic hardening elasto-plastic models which were extensions of the so-called two-surface concept,

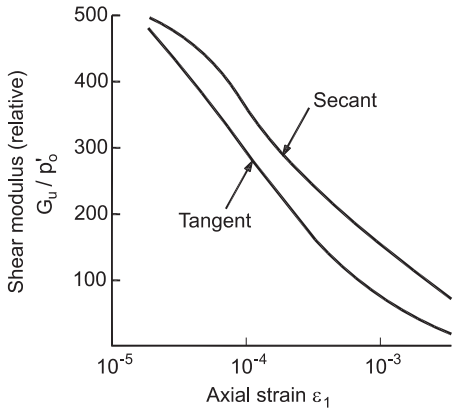


**Figure 1.**
**Comparison of relative secant and tangent shear moduli as dependent on axial strain (after Smith et al. [50])**

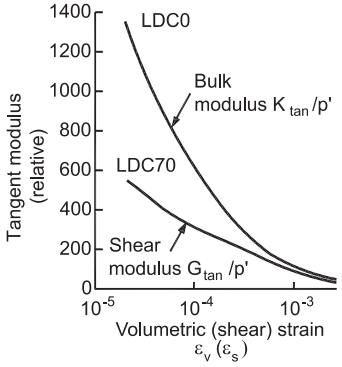


**Figure 2.**
**Variations of tangent bulk modulus with increase of volumetric strain and of tangent shear one with increase of distortional strain (results of drained tests along hydrostatic stress path and stress path of tg70° slope – after Smith et al. [50])**

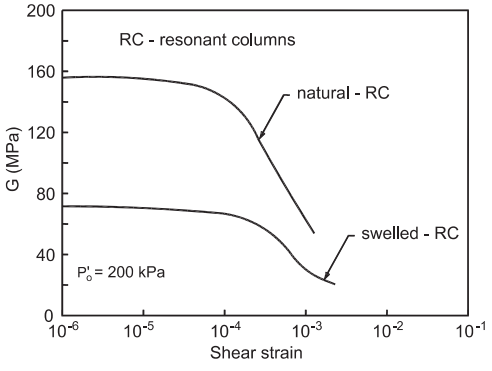


**Figure 3.**
**Variation of shear modulus with distortional strain – results of resonant column tests on Todi clay (carried out by Georgiannou et al. [16])**

and its one – surface simplification in which an elastic area is reduced to a point.

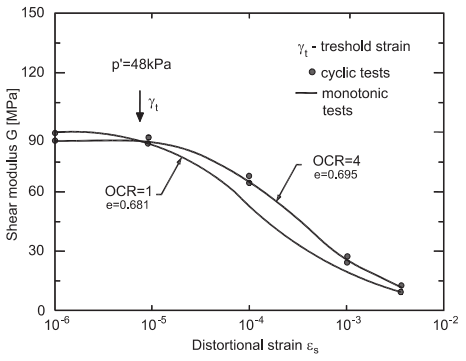


**Figure 4.**
**Effect of the loading character on the shear modulus – comparison of results of cyclic and monotonic tests on Toyura sand (after Burghignoli et al. [5])**

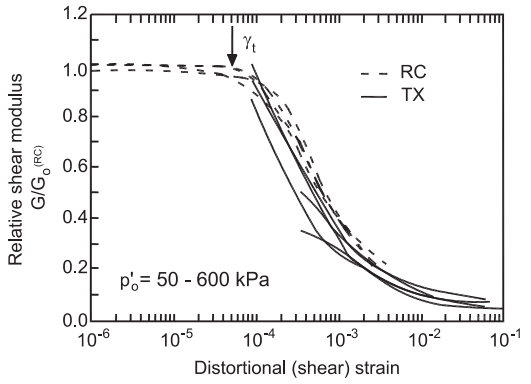


**Figure 5.**
**"Distortional strain-shear modulus" relationship – results of combined resonant column and triaxial tests (after Georgiannou et al. [16])**

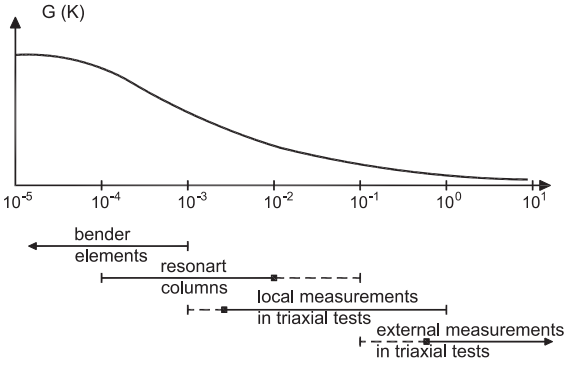


**Figure 6.**
**Approximate ranges of reliable strain measurements techniques for evaluating soil stiffness characteristics**

## 2. EXPERIMENTAL INVESTIGATIONS ON THE SMALL STRAIN STIFFNESS

Experimental observations of overconsolidated soil behaviour at small strains began in the seventies with the laboratory tests in resonant columns [22], [23], [25], [47],. In general, a typical test consisted of the measurement of the velocity of shear elastic wave passing through a soil sample in triaxial or torsional shear apparatus. The goal of the measurement was evaluation of the dynamic shear modulus (as one of the elastic stiffness constants) using the back analysis of the relevant shear wave propagation problem. This parameter appeared to be at least one order of magnitude higher than the commonly known Kirchhoff's modulus for the same soil, evaluated on the ground of results of conventional static triaxial compression or torsional shear tests. Initially, such a great divergence was explained by a difference between material responses to monotonic static and cyclic dynamic loads. However, in the light of results of later investigations the dynamic shear modulus appeared to be constant only in a narrow range of very small strains, estimated as $0 \div 10^{-5}$. According to Hardin and Drnewich [22] the second value is also the upper limit of accurate measurements of the modulus in the resonant column device. The results of tests carried out by the mentioned writers, as well as by Iwasaki et al. [25], showed that this modulus begins to decrease at the value of the distortional strain exceeding $10^{-5}$, initially moderately and then steeply. These results are quoted in Fig. 3.

Independently of that, in the light of the results of parallel laboratory (mainly triaxial compression) tests under monotonic loading at local measurements of deformations, it appeared that the effect of the character of loading on the shear modulus, already insubstantial in the range of deformations $10^{-5} \div 10^{-3}$, can be neglected at very small strains ($<10^{-5}$) [6], [27] (Fig. 4.) Thus, the real reason for the divergence between the "dynamic" and Kirchhoff's moduli appears to be the entirely different ranges of deformations occurring in dynamic and static stiffness tests ($0 \div 10^{-5}$ against $10^{-3} \div 10^{-1}$).

In the face of decreasing the shear modulus with increase of deformations starting from $10^{-5}$, the above facts allow to assume that the "dynamic" and "static" moduli are two values of variable (secant or tangent) shear modulus which is the function of the distortional strain rather than two different elastic constants. This hypothesis has been confirmed by results of numerous laboratory and field tests (see among

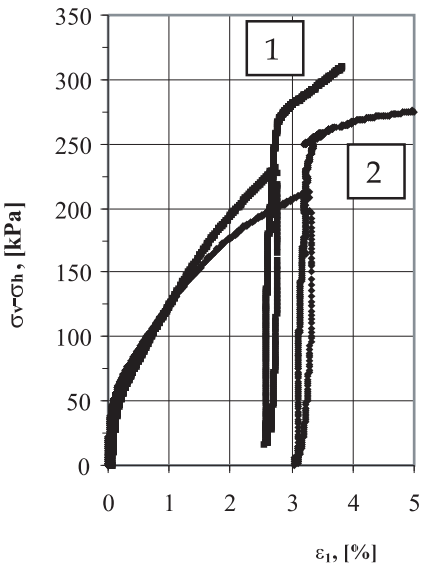


**Figure 7.**
**Divergence of results of external and local measurement of displacements in triaxial apparatus (after Jastrzębska [33])**

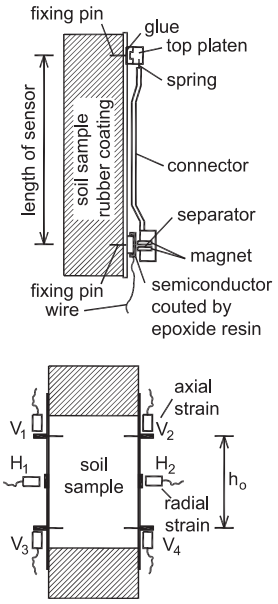


**Figure 8.**
**Two types of gauges for local measurement of displacements in triaxial apparatus, a) Hall effect sensors, b) proximity transducers**

others [6], [16], [28], [42], [43], [56] – and also [2], [5], [7]) Various testing devices and measuring systems (bender elements, resonant columns, triaxial cells with internal local measurement of displacements, conventional triaxial cells with external measurement of displacements) are needed for accurate and convenient measurements in different ranges of strains. Thus, the combined test procedure comprising both ("dynamic" and "static") measurements is, in principle, necessary to identify "distortional strain - secant (tangent) shear modulus" relationship in a wide range of deformation. The good example of such a complete identification are the results of combined investigations (composed of resonant column and triaxial tests) carried out by Georgiannou et al. [16] They are quoted in Fig. 5. Approximate ranges of component measurement techniques situated on the axis of deformations are shown in Fig. 6.

The research tool which played the most important part in studying nonlinear soil behaviour at small strains were drained and undrained triaxial tests with local measurements of microdisplacements. Their results have been interpreted in the form of relationships between distortional strain and shear modulus, axial strain and Young or shear modulus, as well as (only in drained tests) volumetric strain and bulk modulus. Interpretations have comprised secant and tangent moduli. Considering significant inaccuracies in small strain identification using external measuring devices (see e.g. [2], [33], and Fig. 7) studies on the relevant stiffness behaviour had to be proceeded by extensive development and testing of local small strain measurement devices (comp. [9], [17], [29], [32], [33], [35], [39], [55]) Two examples of such gauges are shown schematically in Fig. 8. In their operation the first of them is based on the Hall effect sensors and has been implemented by Clayton and Khatrush [9], while the other uses the proximity transducers and has been applied by, among others, Jastrzębska [33].

Results of studies with triaxial tests using local measurements of microdisplacements and dynamic methods, like those carried out by Georgiannou et al. [16] and quoted in Fig. 5, have been presented by Jardine [28], Jardine et al. [30], Lipiński [35], Porovic and Jardine [42], Powell and Butcher [43], and also Tatsuoka and Shibuya [56.]

Some investigations have been limited to triaxial tests with local measurements of displacements (a.o. Jardine et al. [29], Jastrzębska [32], Smith et al. [50]) This way one cannot, however, measure very small strains to identify the linear elastic soil behaviour in this range.

Special studies, among others by Hardin and Drnewich [22], [23], Jamiolkowski et al. [26], Rampello et al. [46], Viggiani [58], Viggiani and Atkinson [59] have been devoted to this identification, or to be more precise, to evaluation of initial

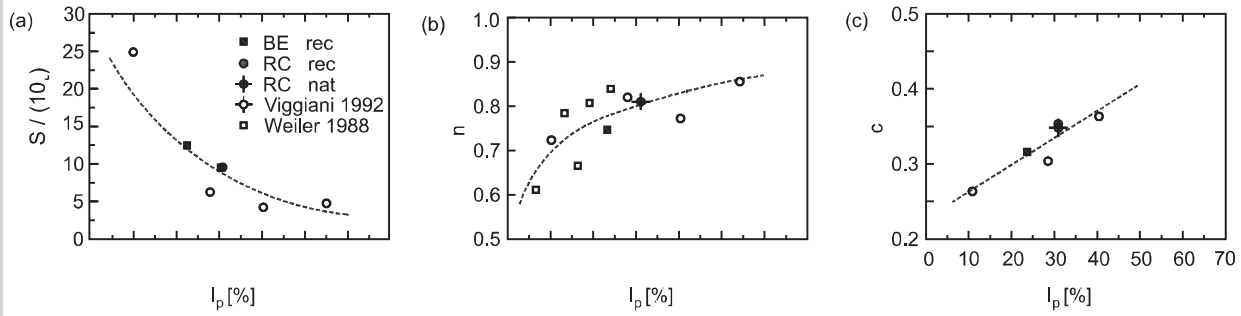


**Figure 9.**
**Stiffness parameters as functions of the index of plasticity $I_p$ (after Rampello et al. [46])**

shear modulus $G_0 = G_{max}$ using, in principle, dynamic methods.

The above studies include, for example, proposals of empirical formulas describing initial shear modulus $G_0$ as dependent on the effective mean stress $p'$, the void ratio $e$ and the overconsolidation ratio $OCR$. The first of them, proposed by Hardin and Black, has been developed by Hardin and Drnevich [23] and has the form

$$G_0 = G_{max} = 1230 \frac{(2.973 - e)^2}{1 + e} (OCR)^K \sqrt{p'} \qquad (1)$$

where $K$ is the material parameter.

Rampello et al. [46] have quoted the Hardin's formula in more general form

$$G_0 = S \cdot f(e) \cdot \left( \frac{p'}{p_a} \right)^n OCR^m \qquad (2)$$

in which $f(e)$ is a function evaluated experimentally, $p_a$ is the atmospheric pressure, and $S$, $m$, $n$ are the material parameters. These authors have also suggested an alternative approach referring to the critical state soil mechanics. Their proposal has the form

$$G_0 = S \cdot p_r^{n} \, p_c'^{(1-n)} \left( \frac{p'}{p_r} \right)^{(n-c)} \qquad (3)$$

where: $p'$ – effective mean stress

$p' = (\sigma_x + \sigma_y + \sigma_z)/3$

$p_c'$ – overconsolidation (equivalent) pressure,

$p_r$ – reference pressure,

$S$, $n$, $c$ – stiffness parameters dependent on the plasticity index $I_p$.

These last parameters have been specified experimentally and shown in the form of correlation curves in Fig. 9a, 9b and 9c.

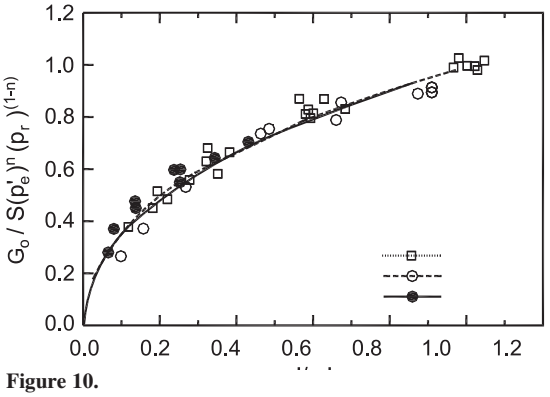


**Figure 10.**
**The normalized "effective mean stress-maximum shear modulus" relationship results of resonant column and bender element tests on Vallerica clay (after Rampello et al. [46])**

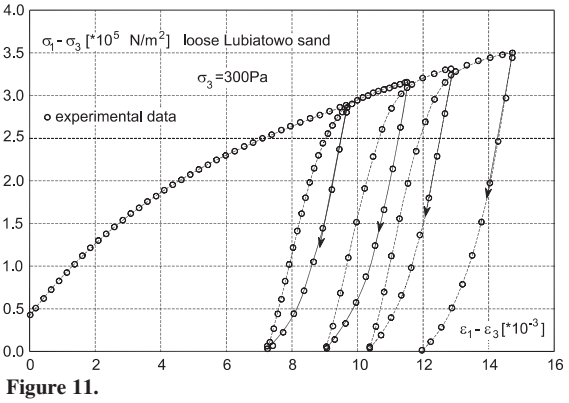


**Figure 11.**
**Shear stress – distortional strain characteristics for several unloading-reloading cycles – results of triaxial tests of loose Lubiatowo sand (after Świdziński [55])**

Fig. 10 presents the normalized "effective mean stress-maximum shear modulus" relationship given by the formula (3) as fitted to experimental data. As can be seen, the parabolic regression is a very close approximation.

Sawicki and Świdziński (see Świdziński [55]) have

proposed an approach to the elastic shear (or Young) modulus evaluation, which is an alternative for the above mentioned dynamic methods using the bender elements or resonant columns. Namely, these researchers have found that an initial straight segment of the unloading branch of "stress-strain" characteristics is longer than its counterpart on the reloading one (see Fig. 11) The segment is sufficiently long for evaluating the maximum shear (or Young) modulus from static triaxial tests with local measurement of strains. An usage of bender elements or resonant columns is no longer necessary. Evaluation of the maximum bulk, Young or constrained moduli using this method presents no difficulty either.

## 3. EXPERIMENTAL INVESTIGATIONS ON THE NATURE OF SMALL STRAIN SOIL BEHAVIOUR

The present section deals with the nature of the small strain nonlinearity and its changes with increasing load. Comprehensive experimental and theoretical studies in this research field have been carried out by Jardine. In his important paper [27] Jardine considers an arbitrary monotonical loading path within the bounding (state boundary) surface, starting from a stable stress point (a local stress origin.) Along this path he distinguishes four stress space zones differing from one another in the nature of soil's deformations (Fig. 12).

Zone *I* is a small area surrounding the starting point where purely linear elastic strains are the only type of deformations to occur. At the same time, the constant values of the moduli within the zone *I* are the maximal ones.

In the light of considerations in [27], the elastic threshold has not been yet quantified precisely. It can be said that the value $10^{-5}$ mentioned in the previous sections is average. Jardine reports $6 \cdot 10^{-6}$ and $2 \cdot 10^{-4}$ as extreme values for Toyoura sand and for London clay respectively. However, after some researchers he also notices in [27] that for slightly overconsolidated soils the zone of purely linear elasticity may not exist.

In the range of very small strains soils can exhibit anisotropic features. Bellotti et al. [4] carried out comprehensive tests evaluating five independent constants in the cross anisotropic linear elastic relationship for dry Ticino silica sand. Generally, the tests consisted in measurements of velocities of various waves passing through a sand specimens of two degrees of density, formed in a large calibration

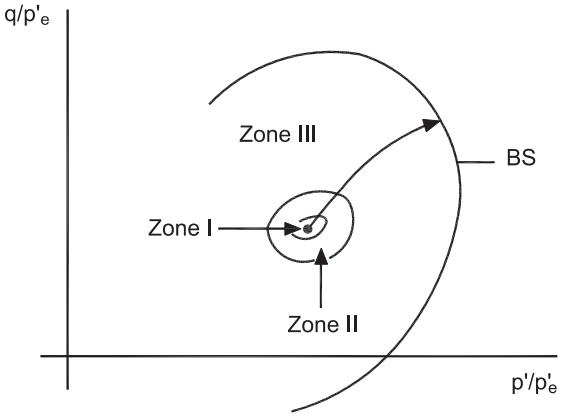


**Figure 12.**
**Zones of the stress space differing in nature of deformations**

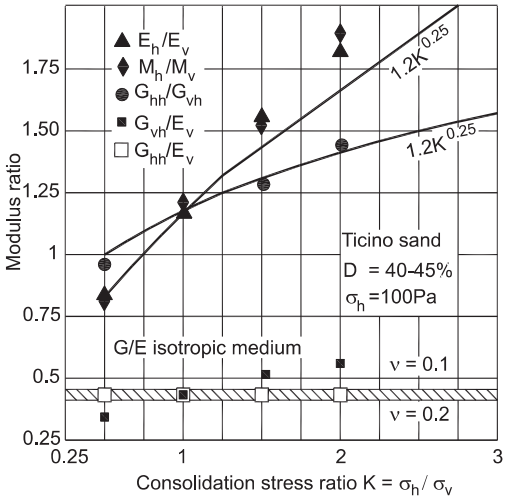


**Figure 13.**
**Effect of consolidation stress ratio on ratios of moduli (after Bellotti et al.[4])**

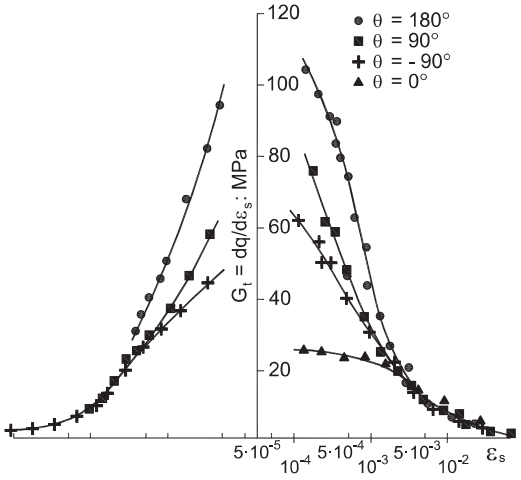


**Figure 14.**
**Effect of recent stress history on stiffness of reconstituted London Clay in triaxial constant p' tests (after Atkinson et al. [3])**

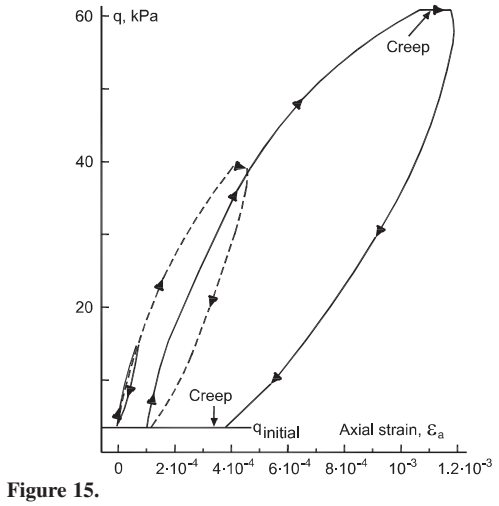


**Figure 15.**
**Stress-strain behaviour in the range of transition from zone II to zone III (results of drained triaxial tests of Magus till-after Jardine)**

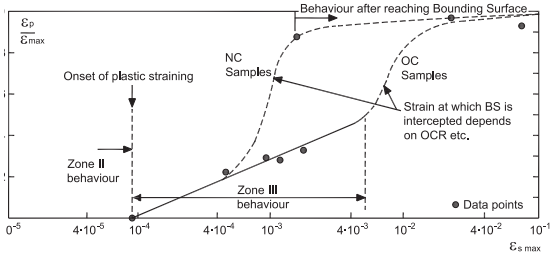


**Figure 16.**
**Variations of the relative permanent shear strain (after Jardine [27])**

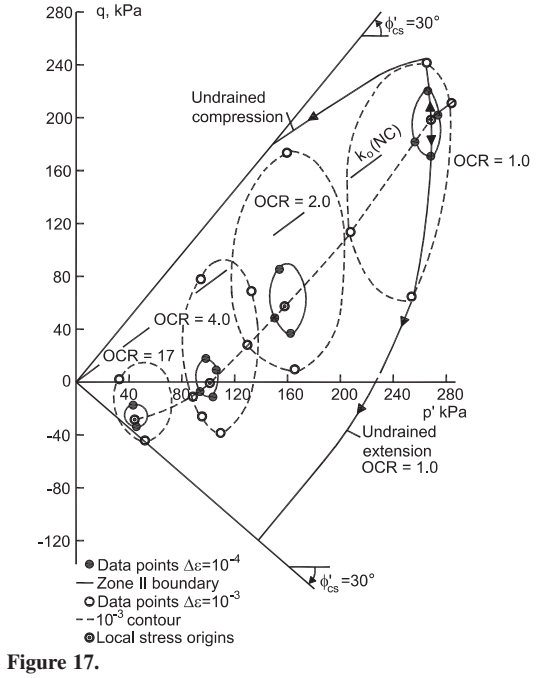


**Figure 17.**
**Boundaries of zones for local stress points lying on the $K_0$ swelling path (after Jardine [27])**

chamber. Constrained compression and shear waves in vertical, horizontal and oblique directions were propagated. The testing procedures were described in detail and many results of tests were presented in [4] (also see Fig. 13).

As in the case of evaluating shear or Young moduli, an alternative approach based on unloading branch analysis has been proposed by Sawicki and Świdziński [48]. They performed triaxial compression tests of Lubiatowo sand, along the hydrostatic and deviatoric stress paths comprising several unloading-reloading cycles. As the result, they obtained four different elastic constants, and this indicates anisotropic soil behaviour. They proved that loose sands are almost isotropic, but for dense sands the anisotropy index differs distinctly from 1.

Once the elastic threshold is crossed, soil begins to behave like material subject to elastic hysteresis. It means that the deformations within the full stress-strain cycle are entirely reversible, although unloading and reloading branches do not coincide, but form closed loops. Jardine [27] interprets the energy dissipation associated with the existence of the hysteretic loop as the result of local microyielding at the inter-particle contacts. The discussed reversible hysteretic soil behaviour occurs in the zone *II* (Fig. 12.) At the same time, soil's response to loading becomes sensitive to recent stress path directions. This phenomenon diminishes gradually, to fade out entirely at strain values of order $2\cdot10^{-3}$ (Fig. 14.) The intensity of changes in stiffness depends on the value of angle $\theta$ of rotation from the previous stress path to the current one in *p'q* space.

Fig. 15 and Fig. 16 demonstrate the essential change in stress-strain behaviour which is related to transition from zone *II* to zone *III* (Fig. 12) after crossing the plastic threshold (about $10^{-5}$ for Toyoura sand and $4\cdot10^{-4}$ for London clay [27]). This change consists in appearance and development of permanent deformations which manifest themselves a.o. by opening (Fig. 15) the loops of hysteresis. Additionally, before and after the plastic threshold, a steep decrease of tangent shear (and bulk) stiffness takes place, as shown in Fig. 5.

Fig. 16 shows path of the relative permanent (plastic) shear strain as dependent on the total strain. In the zone *III*, initially, this quantity grows linearly. Further, this growth becomes progressively nonlinear, to return to previous variability when the stress path reaches the bounding surface (Fig. 16). Then soil becomes normally consolidated and undergoes large plastic strains (zone *IV*).

A particular attention is paid to the boundaries of zones, their extents and shapes [27]. Jardine suggests experimental identification of those by means of adapting one of the two known procedures. The first one consists in performing a suit of drained triaxial tests along the radial stress paths. This way one can find points on the paths corresponding to the plastic threshold of the distortional strain which form the boundary of the zone *II*, and other points which are identified by the strong progression of deformations forming the boundary of the zone *III* and, at the same time, the bounding surface.

The other procedure is an attempt of the direct identification of boundaries of zone *II* and *III*. This consists in performing one consolidation test to the points specified by elastic and plastic threshold of distortional strains and then carrying out undrained compression and extension tests, starting from the above points. This way the main sections of the boundaries are determined. The several remaining points of the boundaries can be established using the first procedure. The extents and shapes of the boundaries in question also depend on positions of the considered stable point in the overconsolidation stress subspace, identified by OCR values. Fig. 17 illustrates the above observations for the case of the $K_0$ swelling path and OCR = 1, 2, 4 and 17.

It is worth noticing that the specification of a sufficient number of suits of the zones' boundaries for various OCR makes a convenient base for numerical specification of the kinematic hardening rule. In Fig. 17 one can also see the quasi-ellipsoidal shapes of the zones. Identification of the boundary of the zone *I* is difficult because stress-strain characteristics at very small strains cannot be measured by means of the triaxial apparatus. Therefore, the boundary of the zone *I* is evaluated as a small area of approximately defined extent and shape.

## 4. SIMPLE CONSTITUTIVE MODELS DESCRIBING SMALL STRAIN NONLINEARITY

The constitutive models for soils, describing the small strain nonlinearity, which are reviewed in the present section, are strictly related to the experimental results presented in Section 2. Namely, the tangent (or in some cases secant), Young, or shear and bulk moduli evaluated experimentally as dependent on stress or strain invariants, make the basic material functions in the mentioned constitutive equations. In terms of the mathematical structure these models can be divided into hypoelastic (nonlinear elastic), and elasto-plastic ones.

The hypoelastic models (defined within the infinitesimal strain theory and formulated in the vectorial notation) have the form of the following incremental matrix equation:

$$\delta\sigma' = \mathbf{D}_t \cdot \delta\varepsilon \tag{4}$$

where the infinitesimal effective stress and strain increments are, respectively,

$$\delta\sigma' = \left\{\delta\sigma'_x, \delta\sigma'_y, \delta\sigma'_z, \delta\tau_{xy}, \delta\tau_{yz}, \delta\tau_{zx}\right\}^T \tag{5}$$

$$\delta\varepsilon = \left\{\delta\varepsilon_x, \delta\varepsilon_y, \delta\varepsilon_z, \delta\gamma_{xy}, \delta\gamma_{yz}, \delta\gamma_{zx}\right\}^T \tag{6}$$

and the tangent matrix of isotropic elasticity

$$\mathbf{D}_t = \begin{bmatrix} K_t + \frac{4}{3}G_t & K_t - \frac{2}{3}G_t & K_t - \frac{2}{3}G_t & 0 & 0 & 0 \\ & K_t + \frac{4}{3}G_t & K_t - \frac{2}{3}G_t & 0 & 0 & 0 \\ & & K_t + \frac{4}{3}G_t & 0 & 0 & 0 \\ & \text{(sym)} & & G_t & 0 & 0 \\ & & & & G_t & 0 \\ & & & & & G_t \end{bmatrix} \tag{7}$$

The most important step in creating hypoelastic constitutive models for soils is the specification of the tangent moduli $G_t$ and $K_t$, or $E_t$ by means of direct approximation (or more precisely – nonlinear regression) of experimental results, such as those shown in Fig. 5. These moduli can also be defined as functions of stress invariants.

The oldest hypoelastic model aimed at accounting for small strain nonlinearity was developed by Duncan and Chang [14]. The tangent modulus $E$, which was the only material function of the model (Poisson's ratio was assumed to be constant), has been adjusted to the description of a standard triaxial test. Therefore, instead the effective mean stress $p'$, the minimal effective principal stress $\sigma_3$ (representing cell water pressure) appeared in the known Duncan-Chang's formula [14]

$$E_t = E' p_a \left(\frac{\sigma'_3}{p_a}\right)^n \left[1 - \frac{R_f q(1-\sin\varphi)}{2(\sigma'_3 \sin\varphi' + c\cos\varphi)}\right]^2 \tag{8}$$

where stress intensity

$q = [(\sigma_x - \sigma_y)^2 + (\sigma_y - \sigma_z)^2 + (\sigma_z - \sigma_x)^2 + 6(\tau_{xy}^2 + \tau_{yz}^2 + \tau_{zx}^2)]^{1/2} / 2.$

Duncan completed the above specification by adding the formula for the bulk modulus $K_t$, [13]:

$$K_t = K^* p_a \left( \frac{\sigma_3'}{p_a} \right)^{n^*} \tag{9}$$

Desai [12] replaced the modulus $E_t$ with the tangent shear modulus $G_t$ in Duncan-Chang formula and applied the effective mean stress $p'$ as the independent variable. The modified relationship has taken the form

$$G_t = G^* p_a \left( \frac{p'}{p_a} \right)^{n^*} \left[ 1 - \frac{R_f (3 - \sin\varphi) q}{6 (p' \sin\varphi + c \cos\varphi)} \right]^2 \tag{10}$$

The tangent bulk modulus $K_t$ completing the matrix $D_t$ can be used in the form (9), but the transition to the effective mean stress is here entirely natural. Thus

$$K_t = K^* p_a \left( \frac{p'}{p_a} \right)^{m^*} \tag{11}$$

In equations (8-11) $E^*, K^*, G, K, R_f^*, R_f, m^*, m, n^*, n$ denote dimensionless material constants, $p_a$ is atmospheric pressure, $\Phi$ is internal friction angle and $c$ is cohesion. The first segment of expression (10), which had referred to the initial shear modulus

$$G_0 = G_{max} = G^* p_a \left( \frac{p'}{p_a} \right)^{n^*} \tag{12}$$

was later replaced by more accurate approximations (2) or (3) proposed by Rampello et al. [46], or similar formulas suggested by Viggiani and Atkinson [59].

A substantial improvement of the small strain stiffness evaluation was achieved in the hypoelastic model developed by Fahey and Carter [15] in which the tangent shear modulus was expressed by formula

$$G_t = G^* p_a \left( \frac{p'}{p_a} \right)^{n^*} \frac{\left[ 1 - f \left( \frac{q - q_0}{q_f - q_0} \right)^g \right]^2}{1 - f (1 - g) \left( \frac{q - q_0}{q_f - q_0} \right)^g} \tag{13}$$

where $q_0$ – initial (in situ) stress,

$q_f$ – critical shear resistance,

$G^*$, n, f, g – material constants.

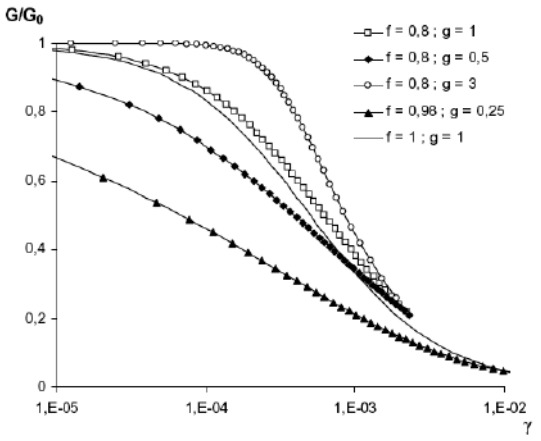


**Figure 18.**
**The comparison of Duncan-Chang's model with Fahey-Carter's one (after [15])**

The formula (10) can be treated as a simple particular case of the expression (13), specified by substituting $q_0 = 0$, $f = R_f$, $g = 1$ and using the Coulomb-Mohr equation for $q_f$.

The relation between both models is clearly shown in Fig. 18 showing the Fahey-Carter's "distortional strain – relative tangent shear modulus" characteristics for various values of parameters $f$ and $g$. The thin line without marked points represents the Duncan-Chang's concept. As can be seen, the Fahey-Carter's proposal offers greater simulative abilities. The first segment of the formula (13) can be improved in a similar manner as previously described, using approximations applied by Rampello et al. [46] or by Viggiani and Atkinson [59].

In his basic paper [27], Jardine mentions a semi-empirical approach in which the simple "stress-tangent modulus" relationships, such as (8), (9), (10), (11), (13), are incorporated into elasto-perfectly plastic or elasto-plastic isotropic hardening constitutive equations for soils, especially into models of critical state mechanics.

These hybrid models constitute the main subject of discussion in the present section. The first group is related to the Fahey-Carter's model. Coquillay [10] has used the formula (13) for definition of $G_t$ in the tangent matrix of elasticity (7) completing its specification by assuming $K_t$ as

$$K_t = \frac{2(1+\nu)}{3(1-2\nu)} G_0 = const. \tag{14}$$

Coquillay has linked the hypoelastic segment of the constitutive matrix equation, quantified by the matrix (7), to the elasto-perfectly plastic component deriving from the plastic flow rule associated with the Coulomb-Mohr limit condition. In [10], Coquillay's model has been implemented to FEM computer code. Some numerical studies have illustrated possibilities of its practical applications.

Another concept has been developed by Gryczmański and Uliniarz [19], [57]. Their proposal was a combination of the well-known concepts: Fahey-Carter model and Modified Cam Clay. The Fahey-Carter model is assumed to be valid within the overconsolidation area, i.e. in the stress subspace confined by the current configuration of MCC yield locus. For normal consolidation states occurring in the remaining physically admissible stress subspace, mechanical soil behaviour is described by the Modified Cam Clay (Fig. 19).

Continuous transition from one model to the other is achieved through treating the bulk and shear moduli as equivalent parameters, differently defined within each of the above mentioned stress subspaces. Assuming Poisson's ratio to be constant, this continuity condition can be expressed by

$$K = \frac{3(1-2\nu)(1+e_0)\left(1-f(1-g)\left(\frac{q-q_0}{q_f-q_0}\right)^{\gamma}\right)}{2(1+\nu)G^{*}p_a\left(\frac{p'}{p_a}\right)^{m}\left(1-f\left(\frac{q-q_0}{q_f-q_0}\right)^{\gamma}\right)^{2}} \qquad (15)$$

Gryczmański-Uliniarz's proposal has been implemented by Uliniarz in the Z_SOIL 7.32 FEM computer code. Fig. 20 presents an essential effect of improvement of MCC by its combination with the Fahey-Carter's model on the run of foundation "load -settlement" curve, particularly for small and medium load values and for heavy overconsolidation.

Biały [5] applied the model proposed by Gryczmański and Uliniarz [19] to the FEM analysis of the large and complex "cooling tower – subsoil interaction" problem. Theoretical responses to loading obtained in [5] exhibit a good qualitative agreement with the results of Burland's field investigations [7]. An example of a fairly good agreement between the FC+MCC model predictions and the results of the measurement of the real cooling tower settlement is quoted after [5] in Fig. 21.

The similar idea of incorporating the empirical formulas into the MCC equations has been implemented independently by Jardine et al. [30], [31].

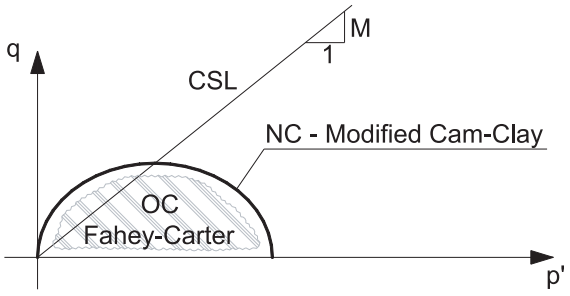


**Figure 19.**
**Graphic representation of FC+MCC model in the p'–q space (after [19])**

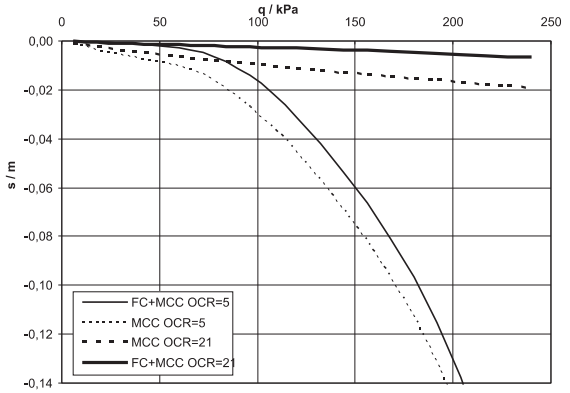


**Figure 20.**
**Comparison of the theoretical load – settlement characteristics for original and improved Modified Cam Clay (OCR = 5 and 20) – after Gryczmański and Uliniarz [19])**

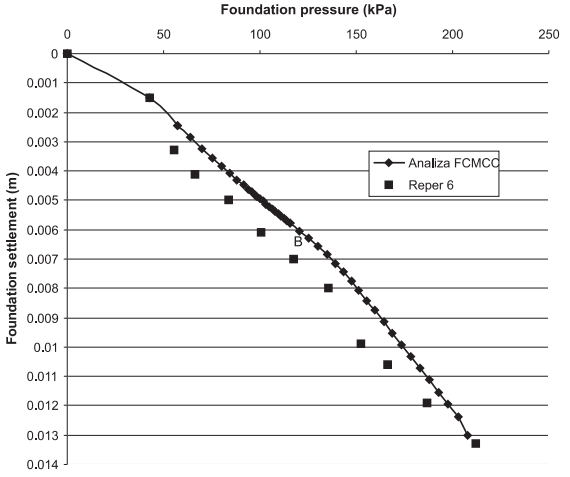


**Figure 21.**
**Predicted and measured settlement of the cooling tower (after Biały [5])**

However, unlike Fahey-Carter's proposal, their description of tangent bulk and shear moduli has the form of a rather complex dependence on volumetric and distortional strains, including trigonometric functions of logarithmic arguments.

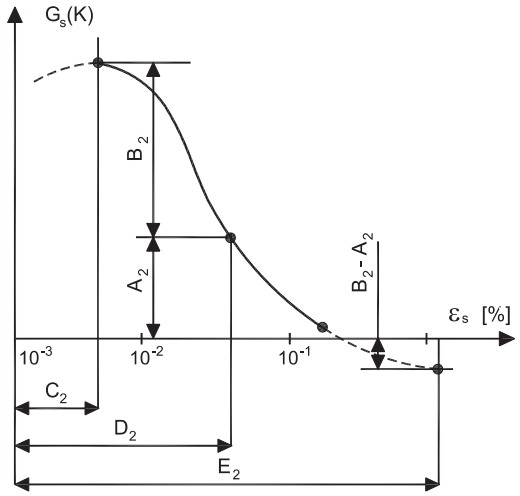


**Figure 22.**
**Physical meaning of parameters in Eq. 16÷19**

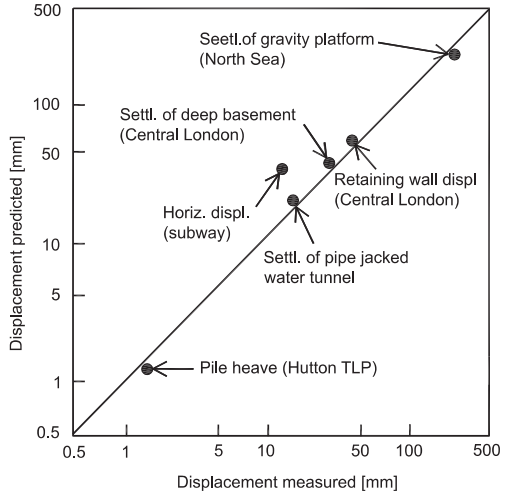


**Figure 23.**
**Displacements predicted using the hybrid model proposed by Jardine et al. [31] against displacements measured for six objects in England (after [31])**

$$K_t = p'\left[A_1 + B_1 \cos(\alpha_1 I_1^{\beta_1}) - B_1 \alpha_1 \gamma_1 I_1^{\beta_1 - 1} \sin(\alpha_1 I_1^{\beta_1})/\ln 10\right] \quad (16)$$

$$G_t = p'\left[A_2 + B_2 \cos(\alpha_2 I_2^{\beta_2}) - B_2 \alpha_2 \gamma_2 I_2^{\beta_2 - 1} \sin(\alpha_2 I_2^{\beta_2})/\ln 10\right] \quad (17)$$

where

$$I_1 = \log(\varepsilon_s / C_1), \qquad I_2 = \log(\varepsilon_s / C_2) \quad (18)$$

$$\alpha_j = \frac{\pi}{2\left[\log(D_j/C_j)^{\beta_j}\right]}, \qquad \gamma_j = \frac{\log 2}{\log\left[\log(E_j/C_j)/\log(D_j/C_j)\right]} \quad (19)$$

$j = 1,2.$

The physical interpretation of some parameters occurring in (16-19) is shown in Fig. 22. Despite various simplifications in the formulation of boundary value problems, not to mention those in the descriptions of the tangent bulk and shear moduli in equations (16-19) FEM analyses performed by Jardine et al. [31] exhibited an astounding agreement of the predicted and measured displacements of eight different civil engineering structures in England (six of them have been quoted in Fig. 23).

## 5. KINEMATIC HARDENING ELASTOPLASTIC MODELS ACCOUNTING FOR SMALL STRAIN SOIL BEHAVIOUR

The conceptual and experimental base for the models reviewed in the present section were investigations concerning the nature of stiffness changes with increasing load, mainly comprehensive studies carried out by Jardine [27]. At this point, it is worth recapitulating the most important properties of overconsolidated soil behaviour which have been observed by Jardine in the range of small to moderate deformations:

1) soil's response to loading is generally inelastic and stress path dependent, except a very small linear elastic region round a stable stress point;
2) there exists an intermediate (adjoining the elastic region) zone where soil's behaviour is of the hysteretic type and dependent on recent stress history, i.e. on the most recent loading path previous to the current state;
3) inelastic stiffness decreases significantly with stretching of any considered loading path, starting from the stable stress point and continuing until the stress reversal happens or the bounding surface is reached;
4) while the stress reversal takes place at any point of the loading trajectory, the stiffness at this new stable point reaches its maximum. Around this point, the small linear elastic region and the intermediate zone *II* of reversible hysteretic soil's behaviour, dependent on recent history form. The stiffness decreases when stresses from the new stable point are withdrawn.

The last observation justifies the concept of the kinematic nature of the overconsolidated soil stiffness and raises the possibility of application of elastoplastic kinematic hardening soil models which are valid in the whole admissible stress space (except for, at most, a very small linear elastic area).

The incremental matrix equation of hypoelasticity (4) for the overconsolidation subspace must therefore be now extended to

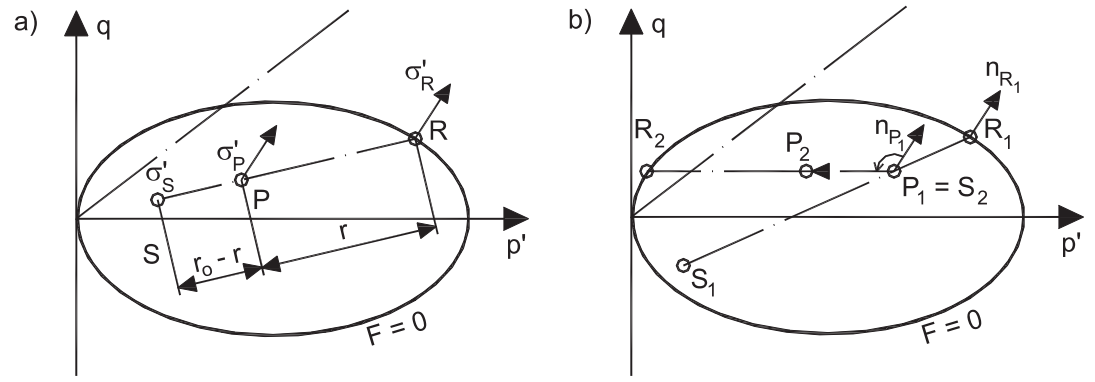


**Figure 24.**
**Radial mapping rule in NAHOS, a) mapping straight line, b) stress reversal (sharp turn of a stress path)**

$$\delta\sigma' = D^{ep} \cdot \delta\varepsilon \tag{20}$$

where the elasto-plastic matrix $\boldsymbol{D}^{ep}$

$$\boldsymbol{D}^{ep} = \frac{\boldsymbol{D} \cdot \boldsymbol{n}_G \cdot \boldsymbol{n}_F^T \cdot \boldsymbol{D}}{\boldsymbol{n}_F^T \cdot \boldsymbol{D} \cdot \boldsymbol{n}_G + K_P} \tag{21}$$

Eq. 21 includes the following vectors and scalars:

– the unit vector $\boldsymbol{n}_F$ normal to the bounding surface $F=0$

$$\boldsymbol{n}_F = \frac{\boldsymbol{a}_F}{\|\boldsymbol{a}_F\|}, \quad \|\boldsymbol{a}_F\| = \left[\boldsymbol{a}_F^T \cdot \boldsymbol{a}_F\right]^{\frac{1}{2}} \quad \boldsymbol{a}_F = \frac{\partial F}{\partial \sigma'} \tag{22}$$

where $a_F$ is the gradient of the bounding surface, and

$\|\boldsymbol{a}_F\|$ – the norm (the length in the stress space) of the gradient vector

– the hardening modulus $\underline{K_P}$ (a general approach)

$$K_P = K_{FR} + K_{int} \tag{23}$$

In Eq. 23 $K_F$ denotes the hardening modulus at the reflecting point on the bounding surface, $K_{int}$ – the increment of the hardening modulus between the current stress point $P$ and the reflecting point $R$.

Here, some explanatory comments may prove helpful. The subscripts $F$ and $G$ in Eq. (21) relate the unit normal vectors and matrices to the bounding surface $F = 0$ and to the corresponding plastic potential one $G^P = 0$ respectively. Most often, surfaces $F = 0$ and $G^P = 0$ are assumed to be identical ($F = 0$) ($G^P = 0$), which implies the plastic flow rule associated with the bounding surface. For description of elasto-plastic behaviour in the overconsolidation area more characteristic surfaces (yield, history, or loading and stress reversal ones) are usually used. Beside the

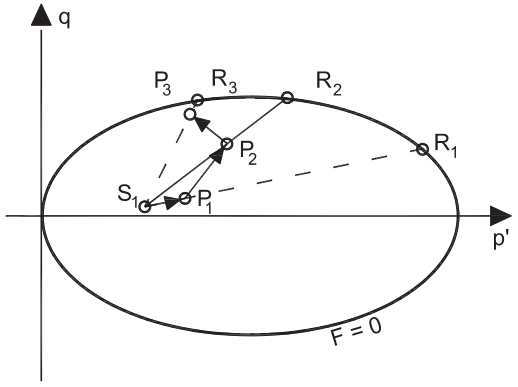


**Figure 25.**
**Functioning of the radial mapping rule for a complex stress path**

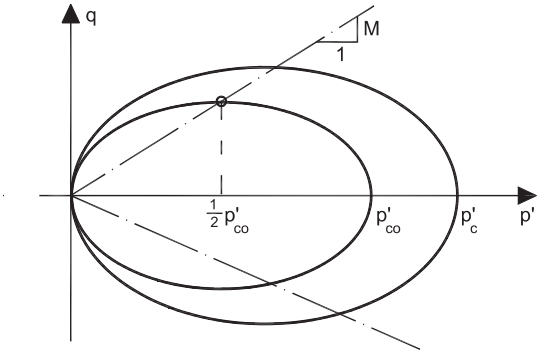


**Figure 26.**
**The standard bounding surface for NAHOS**

Eqs (20)÷(23) related to the bounding surface, analogical equations should refer to every surface on which the current stress point is situated.

In principle, the soil models developed within the kinematic hardening approach, which are to describe realistically small strain phenomena, should take into account all four above-mentioned properties of soil behaviour in the overconsolidation states.

Nearly all of the recently proposed concepts satisfy the above demand. First of all, the three – surface elasto-plastic kinematic hardening models come to mind. However, to achieve a desirable simplicity and computation efficiency, some requirements, such as the existence of two separate zones (*I* i *II*) can be neglected as less important for practical purposes. The remaining requirements have been fulfilled by the one-surface elasto-plastic kinematic hardening model NAHOS developed at the Geotechnical Department of the Silesian Technical University in the period of 1997-2004 by the research team of Jastrzębska, Sternik and Łupieżowiec, under Gryczmański's conceptual leadership. The concepts and results of investigations have been presented in the research reports [20], [21], in the PhD theses [32], [54], [37] and in the contributions to international conferences [34], [35].

The prototype of NAHOS was the author's proposal [18] which represented the Bounding Surface Soil Plasticity (BSSP) family of models originated by Dafalias and Herrmann [11]. It was specified by adapting the empirical formula for tangent Young modulus derived by Jardine et al. [30].

The proper NAHOS is an elasto-plastic kinematic hardening model combining certain elements of Dafalias' BSSP [11] and Hashiguchi's [24] "subloading surface" models. From the first of them NAHOS borrowed the reduction of the linear elastic area to the point (the pole of elasticity) and the general idea of a "radial mapping rule". The latter is the method of evaluation of the hardening modulus field in the overconsolidation subspace (within the bounding surface) using an interpolation technique. The concept consists in extending of the straight line connecting the pole of elasticity *S* with the current stress point *P* to the intersection with the bounding surface (to the reflecting point *R*) – Fig. 24a. In the original BSSP [11] the pole of elasticity is fixed at the origin of the coordinate system.

The modification of the radial mapping rule, following Hashiguchi's concept [24], concerns positioning of the pole of elasticity. In any state of loading of soil element the pole of elasticity is a stable stress point $S_1$, taking a given place in the overconsolidation subspace until the stress reversal (sharp turn of stress path) occurs. Then, the pole of elasticity moves to the stress reversal place and becomes a new stable stress point $S_2$, and the starting point for radial mapping of a new straight line (Fig. 24b) Fig. 25 shows the functioning of the radial mapping rule for the case of a complex stress path.

When a stress path reaches the bounding surface and penetrates its exterior, NAHOS behaves as an elasto-plastic isotropic hardening model. Then, the closed bounding surface undergoes expansion or contraction, together with changes of hardening parameters. The natural selection of a constitutive law for soils are models with volumetric hardening. This places them within the critical state soil mechanics (e. g. [48]).

The original version of NAHOS [20], [21] adapts the Modified Cam Clay yield locus as the bounding surface (Fig. 26). Its equation has the well known form

$$F = q^2 + M^2 p' (p'-p'_c) = 0 \qquad (24)$$

The evolutions of the bounding surface (expansion or contraction) are governed by changes in a permanent part of the void ratio or of the volumetric strain, according to the isotropic hardening law

$$p'_c = p'_{c0} \exp\left(\frac{\Delta \varepsilon_v^p}{\lambda - \kappa}\right) = p'_{c0} \exp\left(\frac{(1+e_0)\varepsilon_v^p}{\lambda - \kappa}\right) \qquad (25)$$

in which $p_{c0}$' is the overconsolidation pressure at the beginning of the loading process. The unit normal vector $\boldsymbol{n}_{FP}$ at any current stress point P is taken as equal to the corresponding vector $\boldsymbol{n}_{FR}$ at the reflecting point on the bounding surface. It follows from the assumption of the existence of the virtual loading surface containing the current stress point and homotetic to the bounding surface. Thus, $\boldsymbol{n}_{FP} = \boldsymbol{n}_{FR}$ while

$$\boldsymbol{n}_{FR} = \left[\frac{1}{3}M^4(2p'_R - p'_c)\boldsymbol{m} + 3\boldsymbol{s}_R\right] / \left[\frac{1}{3}M^4(2p'_R - p'_c)^2 + 6q_R^2\right]^{1/2} \qquad (26)$$

The analytical expression of the radial mapping rule for NAHOS has the general form

$$K_p = K_{pR} + H\left(\sigma'_1, \sigma'_2, \sigma'_3\right)\frac{r}{r_0 - r} \qquad (27)$$

where

$$K_{pR} = \frac{1+e_0}{\lambda - \kappa} M^4 p'_1 p'_R (2p'_R - p'_c) / \left[\frac{1}{3}M^4 p'(2p'_R - p'_c)^2 + 6q_R^2\right] \qquad (28)$$

$$r = \left[ (\sigma'_x - \alpha'_x)^T \cdot (\sigma'_x - \alpha'_x) \right]^{1/2} \quad (29)$$

$$r_0 = \left[ (\sigma'_x - \alpha'_0)^T \cdot (\sigma'_x - \alpha'_0) \right]^{1/2} \quad (30)$$

The form of the hardening function $H$ for the first version of NAHOS (cryptonym NAHOS 1)

$$H = C\left(\frac{r}{r_0 - r}\right)^{\mu} \quad (31)$$

is an attempt of own contribution of the research team to the small strain stiffness description.

The problem of evaluations of the constants $C$ and $\mu$, as well as remaining parameters related to the bounding surface and the isotropic hardening law (see Fig. 27), has been solved by Jastrzębska [32].

To complete the model description an algorithm of determining the reflecting point coordinates must be given. An ingenious, simple way of solving this problem, based on the homotetity of the virtual loading surface and the bounding one, has been given by Sternik [54]. The algorithm has the form

$$\alpha'_R = \alpha'_0 + \beta(\sigma'_p - \alpha'_0) \quad (32)$$

where

$$\beta = \frac{r_0}{r_0 - r} \quad (33)$$

Sternik has also presented a more general equation of the bounding surface accounting for various ellipsoidal shapes controlled by the parameter $R$ and his own computer FEM implementations of the model [54]. As a benchmark of simulative abilities of NAHOS, comparison of the theoretical effective undrained stress paths in $p'q$ space with the triaxial tests results on kaolin samples is presented in Fig. 28. This comparison has been carried out by Sternik [54] who used the results of Kaliakin and Dafalias tests. The compared theoretical and experimental curves in Fig. 28 exhibit a good agreement.

As has already been mentioned, the three-surface elasto-plastic kinematic hardening models constitute the main stream in the development of modeling of soil behaviour at small strains. The first of them has been proposed by Stallebrass [51], [53]. The incremental constitutive equations of the model have been formulated in the triaxial $p'q$ space using the form

$$\begin{Bmatrix} \delta q \\ \delta \varepsilon_v \end{Bmatrix} = \begin{bmatrix} \frac{1}{3G'_c} & \frac{1}{J'_{2c}} \\ \frac{1}{J'_{1c}} & \frac{1}{K'_c} \end{bmatrix} \begin{Bmatrix} \delta p' \\ \delta q \end{Bmatrix} \quad (34)$$

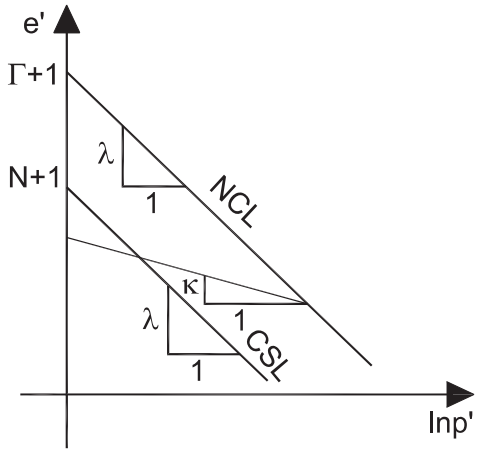


**Figure 27.**
**Parameters specifying the isotropic hardening law in NAHOS**

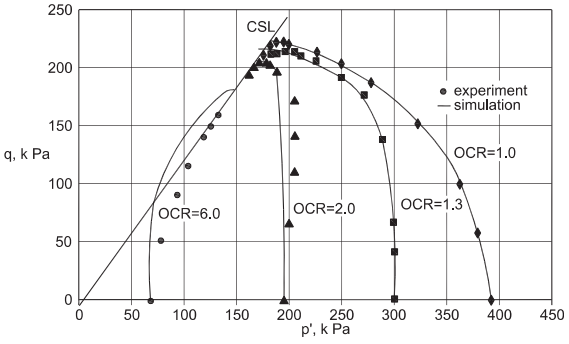


**Figure 28.**
**Comparison of undrained effective stress paths simulated by NAHOS with results of Kaliakin and Dafalias' triaxial tests (after Sternik [54])**

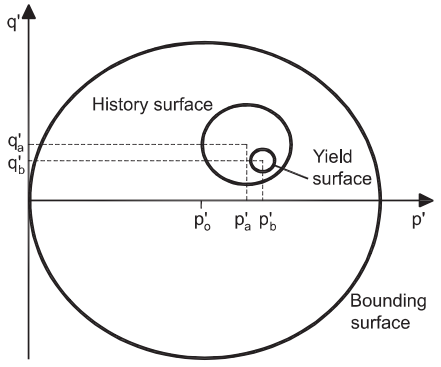


**Figure 29.**
**Three threshold surfaces of three surface Stallebrass' model**

where $K'_c$, $G'_c$ , $J'_{1c}$, $J'_{2c}$ are the tangent bulk, shear and cross-coupling shear and volumetric effects moduli [3]. There are three threshold surfaces in the model which play the key part for its evaluation.

These are (Fig. 29):

– *the bounding surface* $F(p', q, p_0) = 0$ enclosing the admissible stress space and separating the normal consolidation and overconsolidation soil states (specified when describing NAHOS)

$$F = \frac{q^2}{M^2} + (p' - p_0)^2 - p_0^2 = 0 \qquad (35)$$

– the history surface $f_h\,(p', q, p'_b, q_b) = 0$ enclosing the zone *II* discussed in Chapt. 3 within which soil behaviour is of the hysteretic type and is very sensitive to recent loading history,

$$f_h = \frac{(q - q_b)^2}{M^2} + (p' - p'_b)^2 - r^2 p_0^2 = 0 \qquad (36)$$

– the yield surface $f\,(p', q, p'_a, q_a) = 0$ enclosing the zone *I* discussed in Chapt. 3 within which soil exhibits cross anisotropic linear elastic properties

$$f = \frac{(q - q_a)^2}{M^2} + (p' - p'_a)^2 - r^2 S^2 p_0^2 = 0 \qquad (37)$$

In Eqs (35) – (37) $p_0$ denotes the mean stress coordinate of the centre of the current bounding surface, $p'_a$, $q_a$ – the coordinates of the centre of the current yield surface and $p'_b$, $q_b$ – the coordinates of the centre of the current history surface (Fig. 29.). The symbol S stands for the ratio of the yield surface diameter to the history surface diameter, and $T$ is the analogical relation between the bounding and history surfaces.

The plastic parts of the volumetric and shear strains in the triaxial $p'q$ space can be described by the following general formula

$$\begin{Bmatrix} \delta\varepsilon_v^{(p)} \\ \delta\varepsilon_s^{(p)} \end{Bmatrix} = \frac{4}{K_j} \begin{bmatrix} \left(\frac{\partial F}{\partial p'}\right)^2 & \frac{1}{M^2}\frac{\partial F}{\partial p'}\frac{\partial F}{\partial q} \\ \frac{1}{M^2}\frac{\partial F}{\partial p'}\frac{\partial F}{\partial q} & \frac{1}{M^4}\left(\frac{\partial F}{\partial q}\right)^2 \end{bmatrix} \begin{Bmatrix} \delta p' \\ \delta q' \end{Bmatrix} \qquad (38)$$

The isotropically-kinematic hardening rule predicts the movements of the centers of threshold surfaces of the model. These shifts are associated with the stress path induced by external forces transmitted from a structure at a given point of a soil body. The threshold surfaces must not intersect at any moment of the loading process. They may be, at most, internally tangent. Independently of that, during the whole active loading process outside the elastic area, the current stress point must remain on the threshold surface,

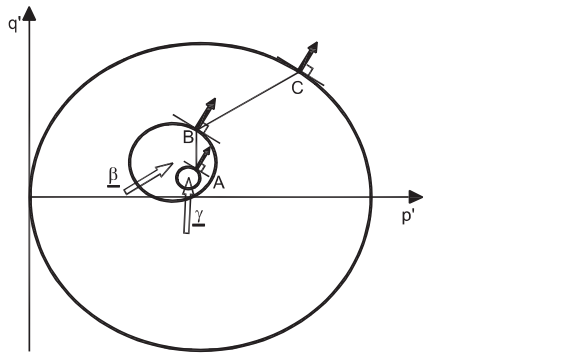


A Current stress state

B, C } Conjugate points with same

γ Vector of movement of yield surface, parallel to AB and of magnitude AB

β Vector of movement of history surface, parallel to BC and of magnitude BC

**Figure 30.**
**Illustration of functioning the translation rule**

and on all nested surfaces, until the unloading process occurs. The above conditions must be fulfilled by the constitutive relations written below.

The yield surface at the current stress point A has the same outward normal as the history surface at the conjugate stress point B (Fig. 30). The rule of translation between points A and B takes the form

$$\begin{Bmatrix} \delta p_a^{(1)} \\ \delta q_a^{(1)} \end{Bmatrix} = R\vartheta \qquad (39)$$

where $R$ is an unknown coefficient, and $\vartheta$ is the vector connecting the points A and B

$$\vartheta = d\vartheta \begin{Bmatrix} p'_B - p'_A \\ q_B - q_A \end{Bmatrix} = \begin{Bmatrix} \frac{p'_A - p'_B}{S} - (p'_A - p'_B) \\ \frac{q_A - q_B}{S} - (q_A - q_B) \end{Bmatrix} \qquad (40)$$

The expansion or contraction of the yield surface related to plastic straining necessitates the correction of the translation rule

$$\begin{Bmatrix} \delta p_a^{(2)} \\ \delta q_a^{(2)} \end{Bmatrix} = \frac{p'_b}{p'_a} \begin{Bmatrix} p'_a \\ q_a \end{Bmatrix} \qquad (41)$$

Finally, the translation rule presents itself as follows

$$\begin{Bmatrix} \delta p'_a \\ \delta q_a \end{Bmatrix} = \frac{\delta p'_B}{p'_B} \begin{Bmatrix} p'_a \\ q_a \end{Bmatrix} + R \begin{Bmatrix} \frac{p'_A - p'_B}{S} - (p'_A - p'_B) \\ \frac{q_A - q_B}{S} - (q_A - q_B) \end{Bmatrix} \qquad (42)$$

Now, it is still necessary to determine the coefficient $R$ making use the consistency condition related to the

yield surface

$$(p'_A - p'_C)(\delta p'_A - \delta p'_C) + \frac{q_A - q_C}{M^2}(\delta q_A - \delta q_C) - T^2 S^2 p'_C = 0 \quad (43)$$

Hence

$$R = \frac{(p'_A - p'_C)\left(\delta p'_A - \frac{\delta p'_C}{p'_C} p'_A\right) + \frac{q_A - q_C}{M^2}\left(\delta q_A - \frac{\delta p'_C}{p'_C} q_A\right)}{(p'_A - p'_C)\left(\frac{p'_A - p'_C}{S} - (p' - p'_C)\right) + \frac{q_A - q_C}{M^2}\left(\frac{q - q_C}{M^2} - q_A\right)} \quad (44)$$

Now, starting from general relations (38), and taking into account the Butterfield's compressibility law [8]

$$\frac{\delta p'}{\delta \varepsilon} = -\frac{1}{\lambda^*}\left(\frac{1+e}{1+e_0}\right)^{\frac{1}{\lambda^*}-1}(1+e_0) \quad (45)$$

having computed the gradients of the yield surface (37) and having performed suitable transformations, the following matrix formula for the increments of plastic volumetric and deviatoric strains can be obtained

$$\begin{Bmatrix} \delta\varepsilon_v^{(e)} \\ \delta\varepsilon_s^{(e)} \end{Bmatrix} = \frac{1}{K_f}\begin{bmatrix} (p' - p'_C)^2 & (p' - p'_C)\frac{q - q_C}{M^2} \\ (p' - p'_C)\frac{q - q_C}{M^2} & \left(\frac{q - q_C}{M^2}\right)^2 \end{bmatrix}\begin{Bmatrix} \delta p' \\ \delta q \end{Bmatrix} \quad (46)$$

where the final form of the equation describing the hardening modulus presents itself as follows

$$K_f = \frac{p' - p'_C}{\lambda^* - \chi^*}\left[p'(p' - p'_C) + q\frac{q - q_C}{M^2}\right] \quad (47)$$

This formula includes two additional components added in order to eliminate infinite strains predicted at certain points of the yield and history surfaces as well as unstable regions of these surfaces.

$$K_f = \frac{1}{\lambda^* - \chi^*}\left[(p' - p'_C)\left[p'(p' - p'_C) + q\frac{q - q_C}{M^2}\right] + \left(\frac{h}{h_{min}}\right)^n p_0 p' + \left(\frac{h}{h_{min}}\right)^n p_0^2\right] \quad (48)$$

Once the stress path has reached the next kinematic surface, i.e. the history one, at the point B (Fig. 30), the yield surface joins with the history surface. They move together in a similar way as previously described, but now the centre of the history surface translates along the vector connecting the current stress point on this surface to the conjugate stress point C on the bounding surface. Finally, when the stress path penetrates the exterior of the latter, the 3-SKH is identified with Modified Cam Clay, and all three surfaces join together. Now, the unloading stress path begins to drag the yield and then the his-

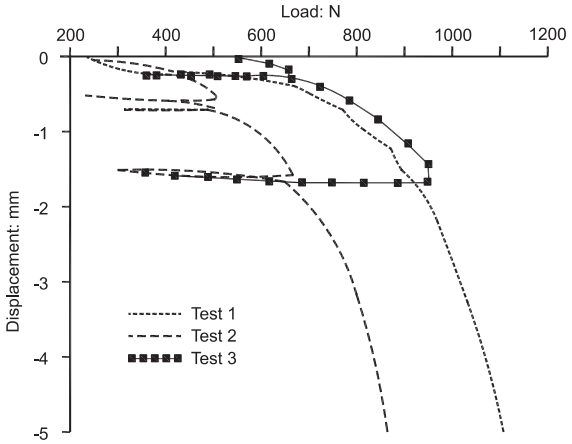


**Figure 31.**
**Comparison of "load-settlement" curve predicted by using 3-SKH model with results of centrifuge tests**

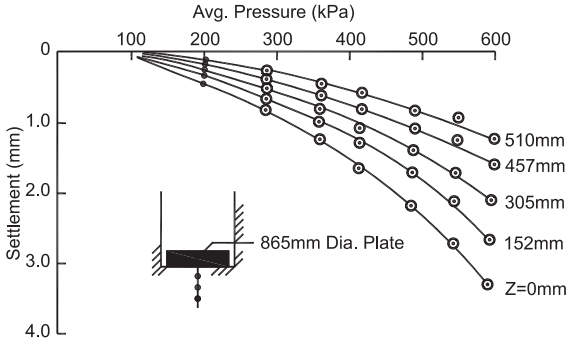


**Figure 32.**
**Load – settlement characteristics on various depths – results of trial plate loading tests (after Burland [7])**

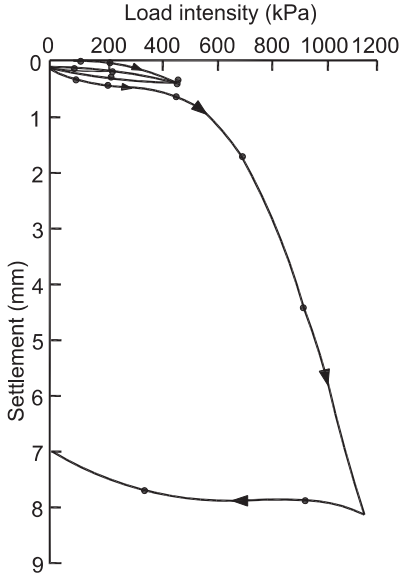


**Figure 33.**
**An example of the steep drop of stiffness resulting in the highly progressive increase in settlement**

tory surface back, in the direction opposite to that shown in Fig. 30. It is worth emphasizing the ability of the model to simulate correctly the effects of the recent history i.e. the rotation from the previous stress path to the current one. This ability is achieved through the concept of an additional history surface (see Fig. 30).

An example of the simulative ability of the 3-SKH model has been presented in Fig. 31. It shows how the model's numerical simulations fit well with results of the centrifuge tests (the case of the test 3).

Two other proposals of three-surface models should also be mentioned. First of them, developed by Puzrin and Burland [45], is based, like the Stallebrass' proposal [51], [53] discussed previously, on the general Jardine's concept of zones of soil behaviour at small strain. Puzrin and Burland also introduce regions: LER (linear elastic region), and SSR (small strain region) corresponding to zones *I* and *II*. The difference between Puzrin-Burland's approach and Stallebrass' proposal consists essentially in different conceptions of zone *II*. Puzrin and Burland assume a nonlinear elastic response of the soil to strains in this region making use of the logarithmic interpolation law [44] developed by them earlier. Other characteristic features of the discussed model are a cross anisotropy of soil within LER and ellipsoidal boundaries of zones. Authors evaluate and verify their proposal on the basis of experimental data for Bothkennar clay [50] exhibiting good agreement of compared results.

The direct improvement of 3-SKH model is the McDowell and Hau's contribution [38].

These authors introduce to the Stallebrass' proposal the non-associated flow rule and their own shape of deviatoric contour of failure surface. McDowell and Hau also prove that their innovations prevent over – predictions of the coefficient of earth pressure at rest for normal consolidation and enable more realistic predictions of responses to cyclic loading.

## 6. CONCLUSION

The present overview does not exhaust this very broad subject matter. Some experimental results and relevant constitutive models have been merely mentioned. The wide interest of geotechnical researchers and engineers in the issues of soil behaviour at small strains stems from scientific aspirations to explore further these exceptionally complex phenomena. The main reason for that interest is, however, the great practical importance of strong physical non-linearity which manifests itself by an abrupt drop of soil stiffness.

There are several very significant effects of the above mentioned property. The first of them, and the most important one, is the influence of discussed non-linearity on the foundation settlement. Some important experimental data are included in the Burland's study [7].

In Fig. 32 the load – settlement curves from trial plate loading tests presented by Burland [7] are quoted. The mentioned non-linearity manifests itself by the ratio of settlement measured to that predicted within the linear elasticity. If an approximate range of the linear elasticity is evaluated as 300 kPa, the minimal value of ratio amounts to about 0.3.

Fig. 33 presents an example of the abrupt drop in stiffness within a narrow range of moderate strain. This phenomenon results in the progressive increase in settlement within the above mentioned range.

Another example of small strain effects can be the intensity of the reduction in the vertical displacement of subsoil beneath the testing plate with the increasing depth. It follows from Fig. 32 that on the depth equal to 0.6 of the plate diameter the measured displacement makes ca 0.36 of settlement of the plate, while the corresponding ratio predicted for the linear elastic halfspace amounts to 0.62, i.e. about 1.7 times more. The effect of non-linearity is therefore the more pronounced reduction in the vertical displace,ment with increasing depth. This effect is particularly evident under diaphragms, such as geogrids or geomattresses. An effective solution to these and other practical boundary value problems which accounts for the effects of the small strain nonlinearity is yet to be found.

## REFERENCES


[1] *Al-Tabaa A., Wood D.M.*; An experimentally based bubble model for clay, Proc. Int. Symp. Num. Models in Geomech. "MUMOG 3", Innsbruck 1989, Elsevier, p.91-99

[2] *Atkinson J.H., Sallfors G.*; Experimental determination of stress-strain time characteristics in laboratory and in situ tests, Proc. 10th ECSMFE, Firence 1991, A.A. Balkema, Rotterdam, Vol.3, p.915-956

[3] *Atkinson J.H., Richardson D., Stallebrass S.E.*; Effect of recent stress history on the stiffness of overconsolidated soil, Géotechnique, 40 (4), 1990, p.531-540

[4] *Bellotti R., Jamiołkowski M., Lo Presti D.C.F., O'Neil D.A.*; Anisotropy of small strain stiffness in Ticino sand, Géotechnique, 46(1), 1996, p.115-131

[5] *Biały M.*; Three-dimensional analysis of a cooling tower foundation with nonlinearly deformable subsoil accounting for the superstructure stiffness, PhD thesis, Politechnika Śląska, Gliwice 2008 (in Polish)

[6] *Burghignoli A., Pane V., Cavalera L.*; Monotonic loading, General Report, Proc. 10th ECSMFE, Firence 1991, A.A. Balkema, Rotterdam, Vol.3, p. 961-979

[7] *Burland J.B.*; Small is beautiful – the stiffness of soils at small strains, 9th Bjerrum Memorial Lecture, Canadian Geotechnical Journal, 26 (4), 1989, p.499-516

[8] *Butterfield R.*; A natural compression law for soils (an advance on e – log p'), Tech. note, Géotechnique, 29(3), 1079, p.469-480

[9] *Clayton C.R.I. , Khatrush S.A.*; A new device for measuring local axial strains in triaxial specimens, Géotechnique, 36(4), 1986, p. 599-603

[10] *Coquillay S.*; Prise en compte de la nonlinearite du comportement des sols soumis á de petites deformations pour le calcul des ouvrages géotechniques, These présentée pour l´ obtention du grade de Docteur de L´Ecole Nationale des Ponts et Chaussées, Specialite Géotechnique, LCPC, Paris 2005

[11] *Dafalias Y.F., Herrmann L.R.*; A bounding surface soil plasticity model, Proc. Int. Symp. Soils under Cycl. Trans. Load., Swansea 1980, p.335-345

[12] *Desai C.S.*; Constitutive laws for geologic media, "Numerical Methods in Geotechnical Engineering", Chapt. 2, Mc Graw Hill, New York 1977, p.65-115

[13] *Duncan J.M.*; Hyperbolic stress-strain relationships, Proc.of the Workshop on Limit Equilibrium, Plasticity and Generalized Stress-Strain in Geotechnical Engineering, Mc Gill University, ASCE, New York 1980, p.443-468

[14] *Duncan J.M.,Chang C.-Y.*; Nonlinear analysis of stress and strain in soils, Journal of Soil Mechanics and Foundations Div. ASCE, 96, SM5, 1970, p.1629-1653

[15] *Fahey M., Carter J.P.*; A finite element study of the pressuremeter in sand using a nonlinear elastic plastic model, Canadian Geotechnical Joumal, Vol.30, 1993

[16] *Georgiannou V.N., Rampello S., Silvestri F.*; Static and dynamic measurements of undrained stiffness on natural overconsolidated clays, Proc. 10th ECSMFE, Firence, p.91-95

[17] *Goto S., Tatsuoka F., Shibuya S., Kim Y.S., Sato T.*; A simple gauge for local small strain measurements in the laboratory, Soils and Foundations 31(3), 1991, p.169-180

[18] *Gryczmański M.*; A bounding surface soil plasticity with a small deformation non-linearity, Compt.Rend. 6-eme Colloque Franco-Polonais de Mec. Sols Appl., Douai 1993, p.146-155

[19] *Gryczmański M., Uliniarz R.*; A simple critical state model with small strain non-linearity for overconsolidated soils, Foundations of Civil Engineering

[20] *Gryczmański M., Jastrzębska M., Sternik K.*; One-surface elasto-plastic model for clay with strongly nonlinear anisotropic hardening – calibration and numerical implementation [in Polish], BK-254/RB-7/98, Politechnika Śląska, Gliwice 1998

[21] *Gryczmański M., Jastrzębska M., Sternik J.*; One-surface elasto-plastic model for clay with strongly nonlinear anistotropic hardening NAHOS 1- verification and application in analysis of geotechnical problems (in Polish), BK-237/RB-7/99, Politechnika Śląska, Gliwice 1999

[22] *Hardin B.O., Drnevich V.P.*; Shear modulus and damping in soils: measurement and parameter effects, Journal of Soil Mechanics and Foundations Div.ASCE, 98 (SM6), 1972, p.603-623

[23] *Hardin B.O., Drnevich V.P.*; Shear modulus and damping in soils: design equations and curves, Journal of Soil Mechanics and Foundations Div.ASCE, 98 (SM7), 1972, p.667-692

[24] *Hashiguchi K.*; A mathematical description of elasto-plastic deformation in normal-yield and sub-yield states, Proc. Int. Symp. Num. Models in Geomech. "NUMOG 2" , Ghent 1986, p.17-24

[25] *Iwasaki T., Tatsuoka F., Takagi Y.*; Shear moduli of sands under cyclic torsional loading, Soils and Foundations,18(1), 1978, p.39-56

[26] *Jamiolkowski M., Lancellotta R., Lo Presti D.C.F.*; Remarks on the stiffness at small strains of six Italian clays, Proc. Int. Symp. "Pre-failure Deformation Characteristics of Geomaterials-Measurement and Application", Is-Hokkaido, Sapporo 1994

[27] *Jardine R.J.*; Some observations on the kinematic nature of soil stiffness, Soils and Foundations, 32(2), 1992, p.111-124

[28] *Jardine R.J.*; Characterising soil behaviour at small to moderate strains, Keynote Lecture, Proc. Int. Symp.

”Pre-failure Deformation Characteristics of Geomaterials – Measurement and Application”, Is-Hokkaido, Sapporo 1994

[29] *Jardine R.J., Symes M.J., Burland J.B.*; The measurement of soil stiffness in the triaxal apparatus, Géotechnique, Vol. 34(2), 1984, p.183-198

[30] *Jardine R.J., Potts D.M., Fourie A.B., Burland J.B.*; Studies of influence of non-linear stress-strain characteristics in soil – structure interaction, Géotechnique, 36(3), 1986, p.377-396

[31] *Jardine R.J., Potts D.M., St. John H.D., Hight D.W.*; Some practical applications of a non-linear ground model, Proc. 10th ECSMFE, Firence, p.223-228

[32] *Jastrzębska M.*; Calibration and verification of the one-suface elasto-plastic model for soils with strongly nonlinear anisotropic hardening, PhD thesis, Politechnika Śląska, Gliwice 2002, (in Polish)

[33] *Jastrzębska M.*; Measurement of small strain in the Geotechnical Laboratory of the Silesian Technical University against background of world achievements [in Polish], Mat. 13 KKMGiF, Gliwice – Szczyrk 2003, Zesz. Nauk. Pol. Śl., Budownictwo, 97, p.13-22

[34] *Jastrzębska M., Łupieżowiec M.*; The effect of the rate on the cyclic strains in the cohesive soils in the light of theoretical and laboratory tests, Proc. 16th ICSMGE, Osaka, 2005, p.807-810

[35] *Jastrzębska M., Sternik K.*; Application of elasto-plastic model with anisotropic hardening to analysis of cyclic loading of cohesive soil, Proc. Int. Conf. “Cyclic behaviour of soils and liquefaction phenomena”, Bochum 2004, p.41-46

[36] *Lipiński M.*; Undrained response of cohesionless soils to monotonic loading, PhD thesis, Politechnika Gdańska, Gdańsk 2000

[37] *Łupieżowiec M.*; Consistent single surface elasto-viscoplastic model with strong nonlinear anisotropic hardening for cohesive soils, PhD thesis, Politechnika Śląska, Gliwice 2004, (in Polish)

[38] *Mc Dowell G. R., Hau K.W.*; A simple non-associated three surface kinematic hardening model, Géotechnique, 53(4), 2003, p.433-437

[39] *Menzies B.K.*; A computer controlled hydraulic triaxial testing system, Advanced Triaxial Testing of Soil and Rock, ASTM STP 977, 1988, p.82-94

[40] *Mróz Z., Norris V.A., Zienkiewicz O. C.*; Application of an anisotropic hardening model in the analysis of elastoplastic deformation of soils, Géotechnique, 29(1), 1979, p.1-34

[41] *Mukabi J. N., Tatsuoka F., Kohata Y., Tsuchida T., Akino N.*; Small strain stiffness of Plejstocene claysin triaxial comression, Proc. Int. Symp. “Pre-failure Deformation Characteristics of Geomaterials – Measurement and Application”, IS – Hokkaido, Sapporo 1994, p.89-197

[42] *Porovic E., Jardine R.J.*; Some observations on the static and dynamic shear stiffness of Ham River sand, Proc. Int. Symp. “Pre-failure Deformation Characteristics of Geomaterials – Measurement and Application”, IS – Hokkaido, Sapporo 1994, p.25-30

[43] *Powell J. J. M., Butcher A.P.*; Assessment of ground stiffness from field and laboratory tests, Proc 10th ECSMFE, Firence 1991, A.A. Balkema, Rotterdam, Vol.3, p.153-156

[44] *Puzrin A. M., Burland J. B.*; A logarithmic stress-strain function for rocks and soils, Géotechnique, 46 (1), 1996, p.157-164

[45] *Puzrin A. M., Burland J. B.*; Nonlinear model of small strain behaviour of soils, Géotechnique, 48 (2), 1998, p.217-233

[46] *Rampello S., Viggiani G., Silvestri F.*; The dependence of small strain stiffness on stress state and history for fine grained soils: The example of Vallericca clay, Proc. Int. Symp. “Pre-failure Deformation Characteristics of Geomaterials – Measurement and Application”, IS – Hokkaido, Sapporo 1994, p.273-278

[47] *Richart F.E. JR, Hall J. R., Woods R.D.*; Vibrations of soils and foundations, Prentice-Hall Englewoods Cliffs, New York 1970

[48] *Roscoe K.H., Burland J.B.*; On the generalized stress-strain behaviour of “wet” clay, “Engineering Plasticity”, Cambridge University Press, Cambridge 1968, p. 535-608

[49] *Sawicki A., Świdziński W.*; Experimental investigations of elastic anisotropy of sands, Archives of Hydro-Engineering and Environmental Mechanics, 49(1), 2002, p.43-56

[50] *Smith P. R., Jardine R. J., Hight D. W.*; The yielding of Bothkennar clay, Géotechnique, 42 (2), 1992, p.257-274

[51] *Stallebrass S. E.*; The effect of recent stress history on the deformation of overconsolidated soils, PhD Thesis, City University, London 1990

[52] *Stallebrass S. E., Jovicic V., Atkinson J. H.*; Influence of geological history on foundation behaviour, Proc. 11th ECSMFE, Copenhagen 1995, 1, p.265-273

[53] *Stallebrass S. E., Taylor R. N.*; The development and evaluation of a constitutive model for the prediction of ground movements in overconsolidated clay, Géotechnique, 47 (2), 1997, p.235-253

[54] *Sternik K.*; Analysis of effectivity and numerical implementation of the one-surface elasto-plastic soil model with strongly nonlinear anisotropic hardening (in Polish), PhD thesis, Politechnika Śląska, Gliwice 2003

[55] *Świdziński W.*; Determination of elastic moduli of sands from triaxial compression test, Archives of Hydro-Engineering And Environmental Mechanics, 47(1-4), 2000, p.51-73

[56] *Tatsuoka F., Shibuya S.*; Deformation characteristics of soils and rocks from field and laboratory tests, Keynote lecture, Proc. 9th Asian CSMFE, Bangkok 1991, 2, p.101-170

[57] *Uliniarz R.*; Ulepszony model Modified Cam-Clay z silną nieliniowością w obszarze prekonsolidacji według Fahey'a-Cartera, Zesz. Nauk. Pol. Śl., Budownictwo, 111, p.419-425 (in Polish)

[58] *Viggiani G.*; Small strain shear stiffness of fine grained soils, PhD Thesis, City Univ. London 1992

[59] *Viggiani G., Atkinson J. H.*; Stiffness of fine-grained soil at very small strains, Géotechnique, 45 (2), 1995, p.249-265

[60] *Wood D.M.*; Strain dependent moduli and pressuremeter tests, Géotechnique, 40 (3), 1990, p.509-512